Science of the Total Environment 633 (2018) 1198–1205

Contents lists available at ScienceDirect

Science of the Total Environment

journal homepage: www.elsevier.com/locate/scitotenv

Enhanced photoelectrochemical degradation of Ibuprofen and generation of hydrogen via BiOI-deposited TiO_2 nanotube arrays

Hanlin Chen [a,b,g], Yen-Ping Peng [c,*], Ting-Yu Chen [d], Ku-Fan Chen [e], Ken-Lin Chang [f], Zhi Dang [b], Gui-Ning Lu [b], Hongping He [a]

[a] CAS Key Laboratory of Mineralogy and Metallogeny/Guangdong Provincial Key Laboratory of Mineral Physics and Materials, Guangzhou Institute of Geochemistry, Chinese Academy of Sciences, University of Chinese Academy of Sciences, Guangzhou 510640, PR China
[b] School of Environment and Energy, South China University of Technology, Guangzhou 510006, China
[c] Department of Environmental Science and Engineering, Tunghai University, Taichung 40704, Taiwan
[d] Department of Landscape Architecture, National Chin-Yi University of Technology, Taichung 40427, Taiwan
[e] Department of Civil Engineering, National Chi Nan University, Nanto 54561, Taiwan
[f] Institute of Environmental Engineering, National Sun Yat-Sen University, Kaoshiung 804, Taiwan
[g] University of Chinese Academy of Sciences, Beijing 100049, PR China

HIGHLIGHTS

- BiOI-coated TiO_2 nanotube arrays was synthesized by chemical vapor deposition.
- The Ibuprofen removal was evaluated by four oxidation systems.
- Recombination of photogenerated holes and electrons were greatly reduced in a self-designed H-type PEC system.
- The synergetic effect between electrochemical and photocatalytic in photoelectrochemical system was quantified.

GRAPHICAL ABSTRACT

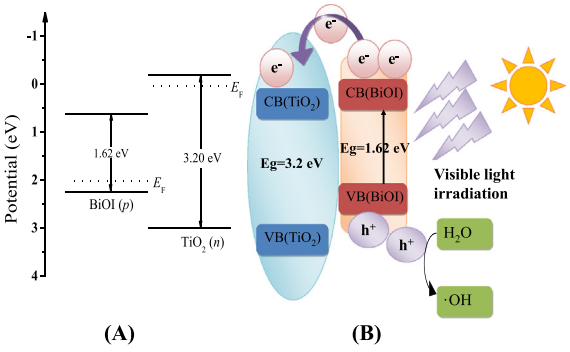

ARTICLE INFO

Article history:
Received 31 January 2018
Received in revised form 22 March 2018
Accepted 22 March 2018
Available online 30 March 2018

Keywords:
Photoelectrochemical
BiOI-TNTAs
Ibuprofen
Synergetic effect

ABSTRACT

This study employed BiOI-deposited TiO_2 nanotube arrays (BiOI-TNTAs) electrode in a photoelectrochemical (PEC) system to oxidize Ibuprofen and generate hydrogen in the anodic and cathodic chamber, respectively. FESEM results revealed the diameter of TiO_2 nanotubes was 90–110 nm. According to the XRD analysis, the BiOI-TNTAs were dominated by the anatase phase and tetragonal structure of BiOI. XPS results confirmed the co-existence of BiOI in the BiOI-TNTAs associated with Bi (33.76%) and I (8.81%). UV–vis absorption spectra illustrated BiOI-TNTAs exhibit strong absorptions in the visible light region. The PEC method showed the best degradation efficiency for Ibuprofen is a rate constant of 3.21×10^{-2} min^{-1}. The results of the Nyquist plot revealed the recombination of photogenerated electron-hole pairs was inhibited as the bias potential was applied. Furthermore, the Bode plot demonstrated the lifetime (τ_{el}) of photoexcited electrons of BiOI-TNTAs was 1.8 and 4.1 times longer than that of BiOI-Ti and TNTAs, respectively. In the cathodic chamber, the amount of hydrogen generation reached 219.94 μM/cm^2 after 3 h of reaction time.

* Corresponding author at: 40704 NO. 181, Section 3, Taichung Port Road, Taichung City 40704, Taiwan.
E-mail address: yppeng@thu.edu.tw (Y.-P. Peng).

https://doi.org/10.1016/j.scitotenv.2018.03.268
0048-9697/

1. Introduction

Titanium dioxide (TiO_2) has been viewed as an efficient, eco-friendly photo-catalyst due to its high photo-activity, photo-stability, low-cost and non-toxicity (Hoffmann et al., 1995; Linsebigler et al., 1995). However, TiO_2 has some innate drawbacks such as a relatively large bandgap (3.2–3.4 eV, only excited by UV light) and fast charge pair recombination, which confines its photocatalytic application.

For the purpose of enhancing the photocatalytic activities of TiO_2, depositing with heterojunction, such as CdS (Cheng et al., 2014; Yao et al., 2014; Yin et al., 2007), Cu_2O (Sun et al., 2016; Talebian et al., 2013), and ZnO (Momeni and Ghayeb, 2015; Tobajas et al., 2016; Yang et al., 2016) etc., is a good way to enhance visible-light absorption and improve charge separation. Among these photocatalysts, BiOI, a *p*-type semiconductor with a forbidden zone of 1.8–2.0 eV, has attracted considerable attention due to its good response in the visible light region. Zhang et al. (2009) first reported the BiOI/TiO_2 heterojunction was synthesized by a simple soft-chemical method and exhibited much higher photocatalytic activity than that of BiOI and TiO_2. However, materials in powder form are difficult to separate and recycle from the reaction system. Highly ordered TiO_2 nanotube arrays (TNTAs) were chosen as a quite effective material for refractory organic compound degradation in the PEC system (Liu et al., 2011a). The highly ordered nanotube array structure makes them an excellent electron infiltration pathway for charge transfer between interfaces (Grimes and Mor, 2009).

The PEC method, combining electrochemical and photocatalytic oxidation, can minimize the hole–electron pair recombination. This method enables various applications, such as solar cells (Peng et al., 2013; Yang et al., 2016; Yu et al., 2015), water reduction (Monfort et al., 2016; van de Krol and Grätzel, 2011; Zhou et al., 2009), CO_2 reduction (Cole et al., 2010; Monfort et al., 2016; Peng et al., 2013) and wastewater treatment (Zhao and Zhu, 2006; Zhang et al., 2007; Peng et al., 2012; Sun et al., 2016). Recently, many research groups have studied the synergetic effect of electrochemical and photocatalytic oxidation and developed good qualitative understanding of the reaction mechanisms (Zhao et al., 2007; Zhao and Zhu, 2006). However, some quantitative information on the synergetic effect in the PEC system is lacking and needed for further understanding.

IBP, an non-steroidal anti-inflammatory drugs (NSAIDs) in the human treatment of fever and pain (Madhavan et al., 2010), has been detected in municipal wastewater treatment plant effluents and natural waters (Camacho-Muñoz et al., 2010) due to its wide use, stability and lack of biodegradation. The concentration of IBP in the environment have been reported to be between 10 ng/L and 160 μg/L (Santos et al., 2007; Skoumal et al., 2009; Méndez Arriaga et al., 2010). Some studies indicated IBP could influence cyclooxygenase reactions and therefore affect not only the reproduction of aquatic animals, but also the photosynthesis of aquatic plants, even in low concentration (Santos et al., 2007; Liu et al., 2015). Therefore, it is urgent to remove these wastewaters before discharging them into the ecosystem.

In this study, BiOI-TNTAs was synthesized by the CVD method and characterized by FESEM, XRD, XPS and UV–vis. BiOI-TNTAs are used as a photoanode in a self-designed PEC system (double-chamber). PEC exhibits strong catalytic activities toward organic contaminant (IBP) degradation and hydrogen generation. In addition, the synergetic effect of electrochemical and photocatalytic in the PEC degradation system was evaluated by electrochemical impedance spectroscopy (EIS) and the Bode plot. The electrochemical properties of the BiOI-TNTAs system and the PEC degradation mechanism of IBP were discussed.

2. Experimental section

2.1. Synthesis of BiOI-TNTAs

Highly ordered TiO_2 nanotubes were fabricated by electrochemical anodization, with the preparation being described in detail in our previous study (Chen et al., 2015). The BiOI-deposited TNTAs were synthesized by the chemical vapor deposition method (CVD). First, 0.05 g BiI_3 (Aladdin Chemistry Co., Ltd.) was added into a ceramic crucible where the obtained TNTAs was laid on. The ceramic crucible was heated to 250 °C at a heating rate of 2 °C/min for 3 h.

2.2. Characterization of BiOI-TNTAs

The crystal structure of samples was elucidated by XRD (X'Pert Pro MRD, PANalytical, Holland) with a Cu Kα source of wavelength 0.154 nm. The morphology was observed with a Nova NanoSEM 430 (FEI, USA) FESEM. The XPS experiments were performed on the TNTAs with a PHI 5000 Versa Probe system (Physical Electronics MN, USA). The binding energy of the XPS spectra was calibrated with reference to the C1s peak 284.8 eV. The UV–vis absorption spectra were measured under the diffused reflection mode using an integrating sphere (UV2401/2, Shimadu, Japan) attached to a Shimadu 2550 UV–vis spectrometer.

2.3. PEC and EC measurements

A three-electrode system was carried out in PEC experiments. A BiOI-TNTAs, a Pt wire and an Ag/AgCl electrode were selected as a working electrode (WE), counter electrode (CE) and reference electrode (RE), respectively. A 100 W Hg lamp was used as the light source in the PEC, PC and P processes. The wavelength of the light sources (Hg lamp) and commercial fluorescent lamp is 365 nm and 450–750 nm, respectively. All degradation experiments were performed in a self-designed H-type reactor, which included a quartz window (7 cm^2), an anode chamber and cathode chamber. These two chambers were connected with a cation-exchanged membrane to maintain the ion balance in the system. Upon light irradiation, the reaction solution was sampled to determine the concentration change of IBP and analyzed by LC (Shimadzu, 64D, Japan). IBP initial concentration was 5 mg/L for all the degradation experiments. The preparation is that 5 mg of IBP was dissolved in water to 1 L in brown volumetric flask and stirred for 7 days. The collected hydrogen gas was detected by gas chromatography (Shimadzu, GC-14B, Japan) with a TCD detector. For comparison, the photocatalytic (PC) experiment was performed using the same system without external potential. An electrochemical (EC) oxidation experiment was performed at the same bias without light illumination.

The I-t curve measurements and PEC degradation experiments were controlled by an electricity workstation (ΩMetrohm-AutoLAB, PGSTAT302N, Holland). EIS tests were performed under open circuit voltage over a frequency range from 10^5 Hz to 10^{-2} Hz with an AC voltage magnitude of 5 mV.

3. Results and discussion

3.1. Characterization of BiOI-TNTAs

The morphologies of the TNTAs, BiOI-Ti and BiOI-TNTAs were characterized by SEM. Fig. 1A displays a typical SEM image of the TNTAs with a regularly arranged pore structure. The TNTAs show an average outer diameter of 105 nm and wall thickness of 20 nm. Fig. 1B and C shows the SEM image of BiOI-Ti and BiOI-TNTAs, respectively. The SEM image illustrates the BiOI scattered on the surface of Ti and TNTAs, and the formed sheet-structure. In addition, Fig. 1C shows the outer and inner pore diameter of the nanotube was about 100 and 80 nm, respectively. This result suggests TNTAs retain their integrity with no significant morphological change after BiOI deposition. The result here is similar to the findings of Dai et al. (2011) who fabricated BiOI/TNTAs by the impregnating hydroxylation method. Notably, the color of the TNTAs film became yellow, implying a thin layer of BiOI film was successfully deposited on the TNTAs surface. EDX analysis of the BiOI-TNTAs is shown in Fig. 1D, indicating the nanocomposites

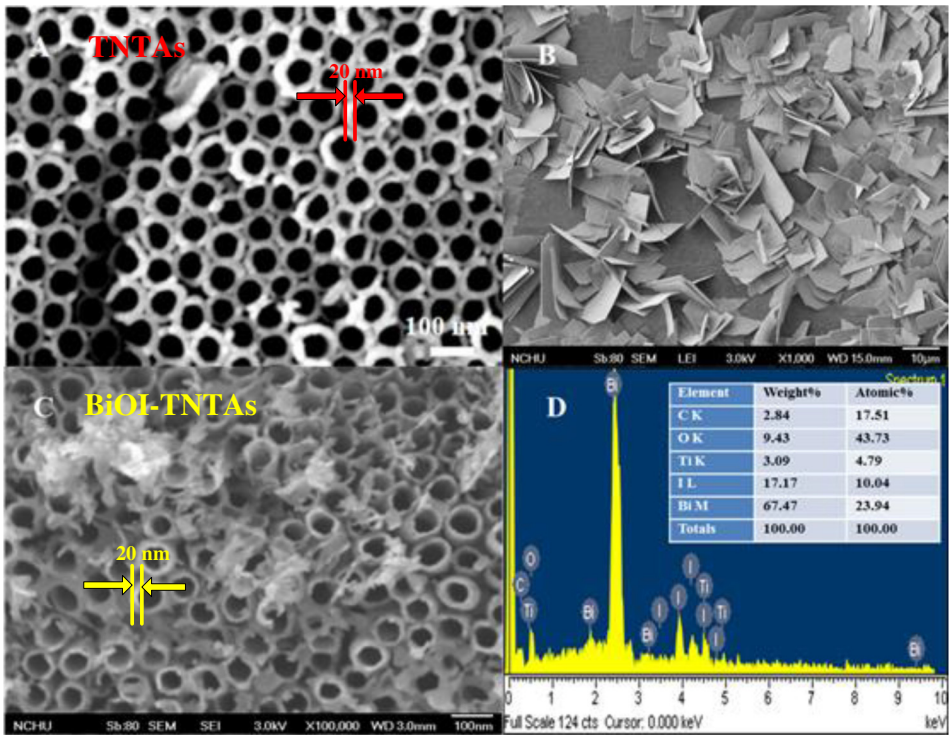

Fig. 1. FESEM images of (A) TNTAs, (B) BiOI-Ti, (C) BiOI-TNTAs and (D) EDX results of BiOI-TNTAs.

contained Ti, O, Bi and I. Furthermore, Table 1 shows that the atomic percent (at.%) of Ti, O, Bi and I is 20.27, 18.25, 33.76 and 8.81%, respectively. These results illustrate the BiOI had successfully deposited onto the TNTAs. Film material, such as BiOI-TNTAs, with high photocatalytic reactivity and strong stability can therefore serve as a photoanode. The TNTAs-based PEC system might perform well as a promising method for wastewater treatment and the present fuel cell system (Liu et al., 2011b). The results of XRD show no other phase beside Ti metal, TiO_2 anatase and tetragonal BiOI phase in the BiOI-TNTAs samples (Fig. S1). The XPS results further confirm the coexistence of BiOI and TiO_2 in BiOI-TNTAs (Fig. S2).

The optical property of BiOI-Ti, TNTAs and BiOI-TNTAs was examined by UV–vis absorption spectra, as shown in Fig. 2. The spectrum obtained from the pure TNTAs film (Fig. 2A) shows TNTAs can be excited under ultraviolet light at a wavelength below 400 nm, which was ascribed to the intrinsic band gap absorption of TiO_2. The absorbance shoulders of pure TNTAs in the visible region can be assigned to the scattering of light caused by pores or cracks in the nanotube arrays (Dai et al., 2011; Yu et al., 2003). In contrast, Fig. 2B reveals the BiOI-Ti and BiOI-TNTAs film show strong absorbance shoulders in the wavelength ranging from 400 to 650 nm and 400 to 630 nm, corresponding to bandgaps of 1.6 and 1.62 eV (can be calculated according to the Tauc formula, $(\alpha h\nu)^{1/2} = \beta(h\nu - E_g)$), respectively. This phenomenon can be assigned to the intrinsic band gap absorption of BiOI that could facilitate the absorption of the solar energy in the visible region.

Table 1
Element content results of XPS analysis for BiOI-TNTAs.

Name	Peak BE[a]	Height counts	FWHM[b] eV	Area (P) CPS	At.%[c]
Bi4f7	158.62	12273.69	1.17	27851.24	33.76
C1s	284.74	537.79	1.37	1120.11	18.9
I3d5	619.11	4049.05	1.36	10099.9	8.81
O1s	529.72	1843.6	1.32	3121.4	18.25
Ti2p3	465.89	1339.51	3.46	6213.76	20.27

[a] BE: binding energy.
[b] FWHM: full width at half maximum.
[c] At.: atom.

3.2. Photoelectrochemical activity of BiOI-TNTAs

IBP degradation by using different materials (TNTAs, BiOI-Ti and BiOI-TNTAs) and methods (P, PC, EC and PEC represent photolytic, photocatalytic, electrochemical and photoelectrochemical, respectively) were compared, as shown in Fig. 3. The light source applied in the PEC, PC and P experiments was a 100 W Hg lamp irradiation. In addition, a bias potential of 1.2 V (vs. Ag/AgCl) was employed in the PEC and EC processes. As shown in Fig. 3A, the PEC process was the most efficient way in degrading IBP. IBP was completely removed in 120 min via the PEC method, whereas only 81.69 and 2.04% of the IBP was removed by the PC and EC processes, respectively. In this study, IBP degradation by the PEC system fits a pseudo-first-order reaction, $\ln(C_0/C) = kt$, where k is the apparent rate constant and C_0 and C are the initial and reaction concentrations of aqueous IBP, respectively. Table 2 shows the rate constants of IBP degradation are 3.21×10^{-2}, 2.13×10^{-2}, 0.02×10^{-2} and 1.81×10^{-2} min^{-1} for PEC, PC, EC and P methods, respectively. IBP PEC degradation by TNTAs, BiOI-Ti and BiOI-TNTAs were also compared. IBP was completely degraded in 120 min by the PEC method using the BiOI-TNTAs photo-anode. Clearly, BiOI-TNTAs performed more efficiently than BiOI-Ti and TNTAs in IBP degradation (Fig. 3B, Table 3). As to the IBP degradation via the PEC, PC, P and EC methods, the TOC removal rates were 55.18%, 40.30, 28.19 and 12.63%, individually (Fig. 3C).

The reusability and stability of IBP degradation and hydrogen generation via BiOI-TNTAs were examined in this study. As shown in Fig. 4, the BiOI-TNTAs PEC degradation of IBP shows high stability in the course of the PEC recycles and retained 100% of its initial activity with the first-pseudo rate constants of 0.0321, 0.034, 0.0316 min^{-1} for three runs (Fig. 4A). Meanwhile, in the cathodic chamber, the amount of hydrogen generation reached 219.94, 207.4, 219.9 μM/cm^2 after a 3 h reaction time for each cycle (Fig. 4B). The results above illustrated

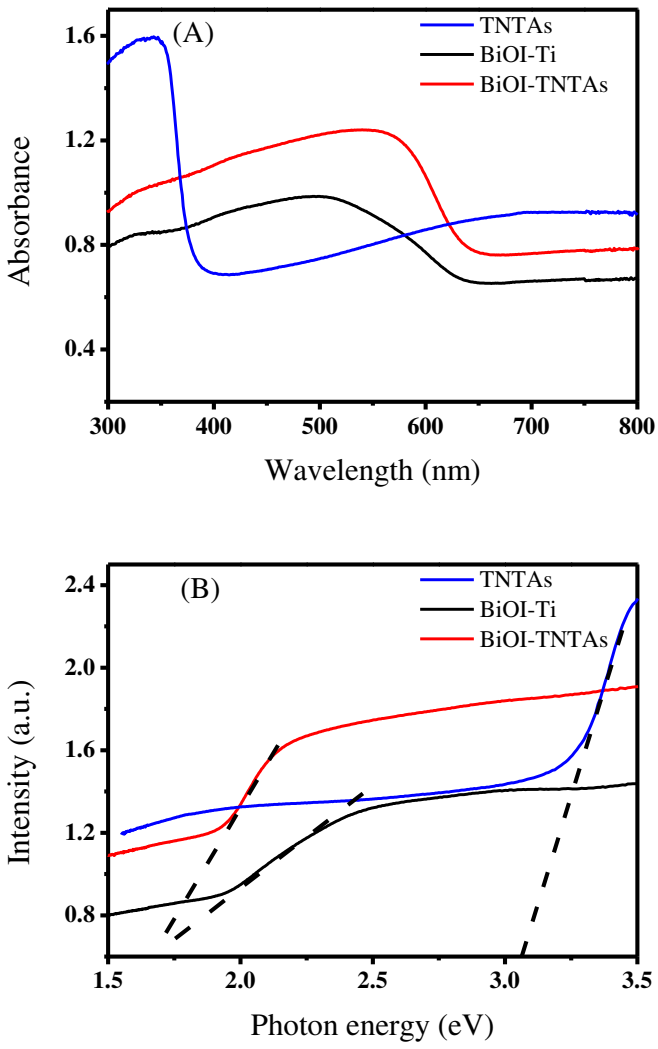

Fig. 2. UV–visible diffuse reflectance spectra of (A) unmodified TNTAs, BiOI-Ti, and BiOI-TNTAs, and (B) their corresponding bandgap plot.

BiOI-TNTAs display good stability and can be reusable. In the PEC system, the applied bias potential can minimize the recombination of photo-generated electrons and holes and thereby enhance the photon-efficiency, enabling simultaneous utilization of photo-generated holes to degrade IBP and electrons to generate hydrogen.

A 13 W commercial fluorescent lamp was selected to compare the light sources. As shown in Fig. S3, 35.9% of the IBP was removed by the PEC method, while merely 5.2% of IBP was removed by commercial fluorescent lamp irradiation. This result demonstrates the visible-light induced PEC applications of BiOI-TNTAs are feasible. Compared to the IBP degradation results in Fig. 3B, the PEC method exhibited better performance under UV-light than visible-light illumination. Although the UV–vis results provide evidence BiOI-TNTAs can be excited in the visible light region, the IBP degradation results showed a better photo-electro response at shorter irradiation wavelength. This might be because irradiation at a shorter wavelength always accompanies higher photo-energy. Higher photo-energy leads to greater photon kinetic energy, facilitating movement of photons.

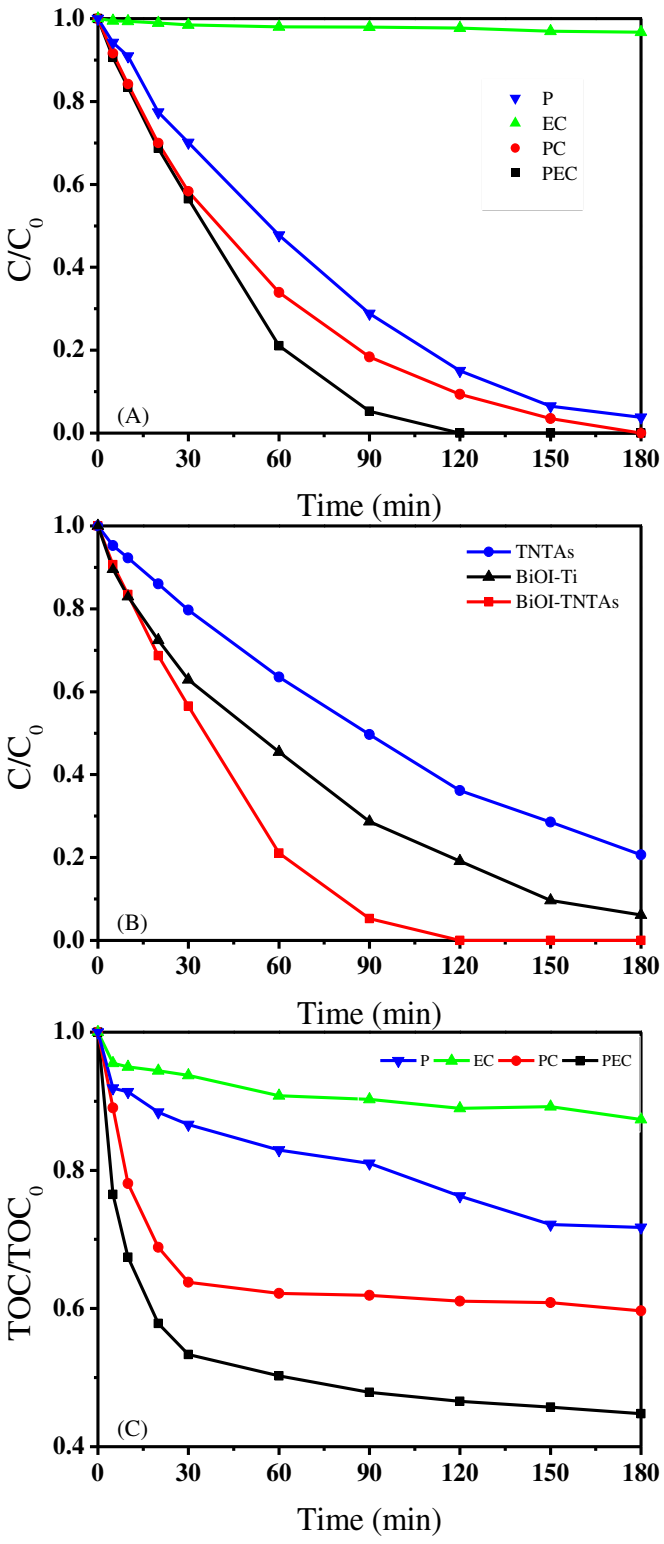

Fig. 3. IBP Degradation by different method (P, PC, EC and PEC) (A), PEC degradation by different materials (B), and TOC removal of Ibuprofen degradation (C). Experiment condition: IBP concentration is 5 mg/L, light source is 100 W low-pressure Hg light.

3.3. Photoelectrochemical properties of BiOI-TNTAs

Electron-hole pairs would be generated as the light illuminated at BiOI-TNTAs photo-anode. Therefore, transient photocurrent responses were conducted to evaluate the photocatalytic performance of the photo-anode. Fig. S4 shows BiOI-TNTAs exhibit the highest photocurrent (0.147 mA), which was 2.8 times higher than that of the TNTAs (0.053 mA), indicating deposition with BiOI significantly enhanced electron mobility by reducing the recombination of electron-hole pairs. Moreover, the photocurrents were enhanced with the increased bias

Table 2
Pseudo-first-order rates of IBP degradation (k_{obs}) under different processes.

Processes	Constant (k_{obs}, min^{-1})	R^2
P	0.0181	0.9835
PC	0.0213	0.9899
EC	0.0002	0.9842
PEC	0.0321	0.9724

Table 3
Pseudo-first-order rates of IBP PEC degradation (k_{obs}) via different materials (BiOI-Ti, TNTAs and BiOI-TNTAs).

Materials	Rate constant (k_{obs}, min^{-1})	R^2
TNTAs	0.0087	0.9967
BiOI-Ti	0.015	0.9922
BiOI-TNTAs	0.0321	0.9724

potential (0 to 1.2 V) in the PEC system (Fig. S5). This result agreed with the finding of Chen et al. (2015), showing the photo-generated electrons would be driven to the cathode as the bias potential was applied in the PEC system. The above results indicated applying a bias potential to the PEC system can attract more electrons to the cathode of BiOI-TNTAs, thereby increasing the photocurrents and leaving more holes to participate in the oxidation reaction in the anodic chamber.

The behavior of the charge transfer processes at the semiconductor–electrolyte interface can be explained by EIS (Cheng et al., 2008; Kang et al., 2013; Ye et al., 2012). Fig. 5A shows the Nyquist plots of BiOI-Ti, TNTAs and BiOI-TNTAs under light illumination. The smaller semicircle arc diameter illustrates a more effective separation of the photogenerated electron–hole pair (Cheng et al., 2008; Kang et al., 2013). The inset plot in Fig. 5A refers to the equivalent circuit plot of the BiOI-TNTAs PEC system. *Rs*, *Rp* and *CPE* represent the resistance of the solution, the resistance to charge transfer at the interface between BiOI-TNTAs and electrolyte, and the constant phase element (Wang et al., 2012), respectively. The fitting results for the equivalent circuits of BiOI-Ti, TNTAs and BiOI-TNTAs are shown in Table 4. Under an applied potential of 1.2 V bias, the *Rp* values for TNTAs, BiOI-Ti and BiOI-TNTAs were 1154.4, 567.26 and 343.32 Ω, respectively. These results reveal electrons transfer faster in the BiOI-TNTAs PEC system than in the TNTAs PEC system. Further, the *Rp* value increased with the bias potential applied (Fig. S6). The results of the EIS analyses are consistent with the findings in I-t (Fig. S5), illustrating the electrons transfer faster with increasing applied bias potential.

Meanwhile, the electron lifetimes (τ_{el}) of the photoexcited electrons for the BiOI-TNTAs PEC system were examined. The values were obtained from the Bode phase plot at a frequency between 10^{-1} to 10^3 Hz according to the following equation (Wang et al., 2012; Ye et al., 2013).

$$\tau_{el} = \frac{1}{\omega_{max}} = \frac{1}{2\pi f_p}$$

Fig. 5B, C and D shows the estimated electron lifetimes of the TNTAs, BiOI-Ti and BiOI-TNTAs were 0.787, 1.833 and 3.238 ms, respectively. The measurements revealed the electron lifetime of the photoexcited

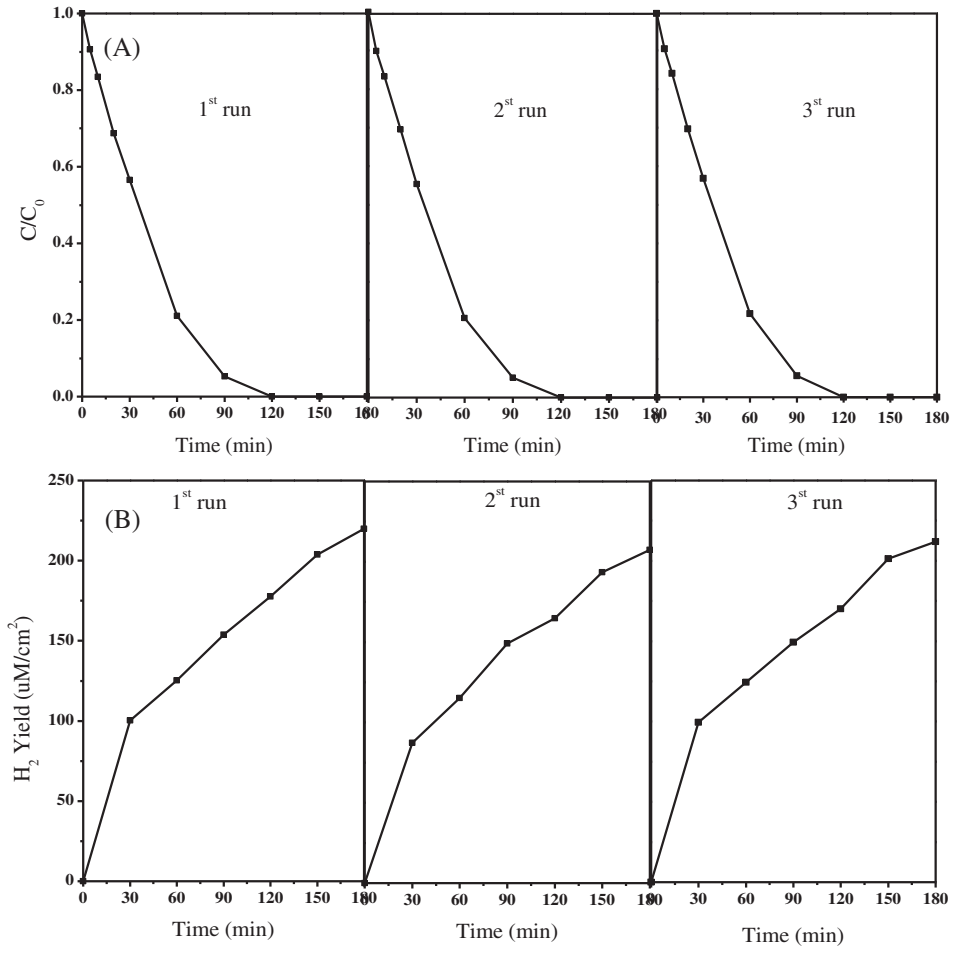

Fig. 4. Cycle runs in the (A) PEC degradation of Ibuprofen and (B) PEC generation of hydrogen (applied voltage = 1.2 V, Ibuprofen concentration = 5 mg/L, light source = 100 W low pressure Hg light).

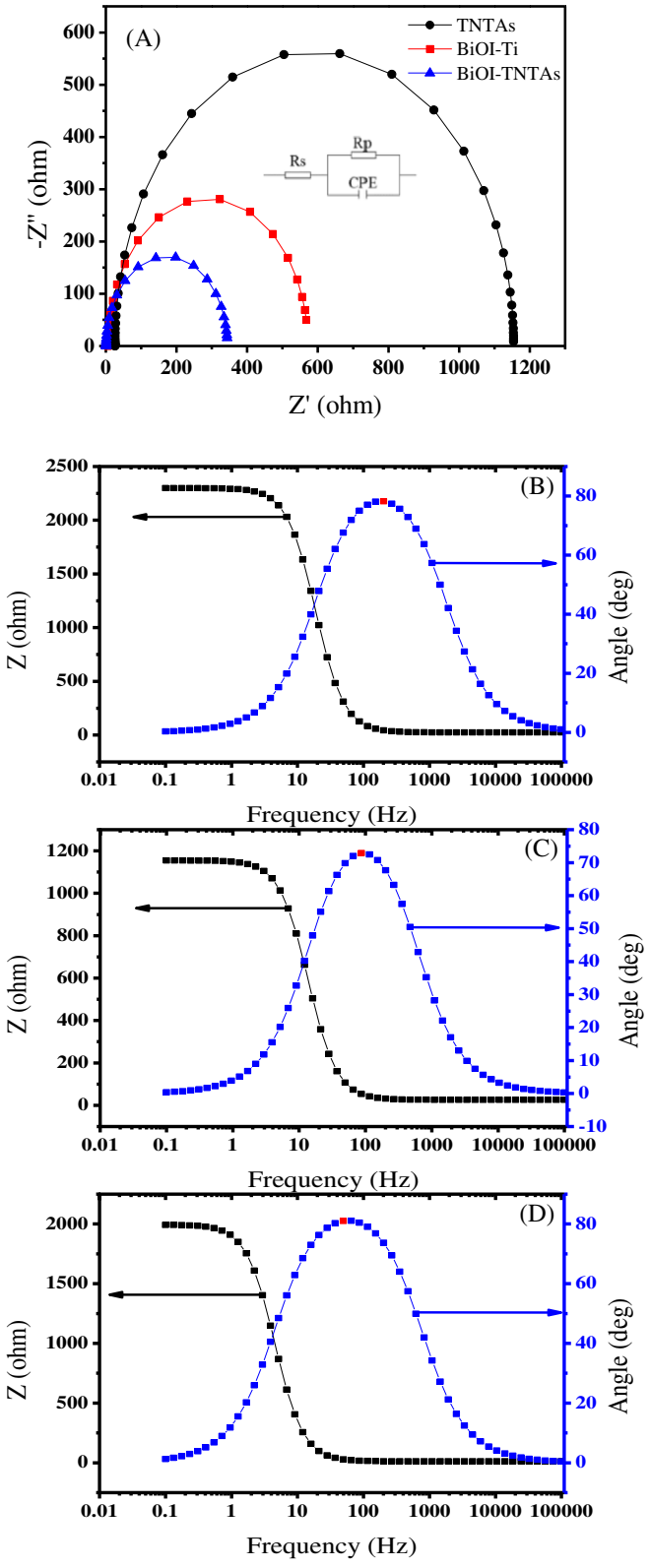

Fig. 5. Electrochemical impedance spectra of samples for Nyquist plot of BiOI-Ti, TNTAs and BiOI-TNTAs (A) and Bode phase plots of BiOI-Ti (B), TNTAs (C) and BiOI-TNTAs (D) at 1.2 V in 0.1 M NaCl solutions under 100 W low-pressure Hg light illumination.

electrons in the photoanodes increased about 4.1 times following BiOI deposition. Similar results can be found in the study of Ye et al. (2013).

Table 4
Fitting results for equivalent circuits of BiOI-Ti, TNTAs and BiOI-TNTAs.

Samples	Rs (Ω)	Rp (Ω)	f_{max} (Hz)	τ_{el} (ms)
TNTAs	26.09	1154.4	202.36	0.787
BiOI-Ti	6.279	567.26	86.85	1.833
BiOI-TNTAs	0.908	343.32	49.41	3.238

3.4. Mechanism of BiOI-TNTAs PEC system

In the PEC system, the photocurrent increased with an external bias potential, leading to reduced recombination of photo-generated holes and electrons. The photo-generated electrons followed the electric field as EC currents, accelerating the separation of electron-hole pairs. The enhanced PEC activity of BiOI-TNTAs can be ascribed to the synergetic effects of the photochemical and electrochemical and *p-n* junction structure (Zhang et al., 2009). The photocatalytic activity depends on the electron-hole pairs generated by BiOI-TNTAs with light irradiation. The photo-generated electrons and holes could transfer to the surface of the BiOI-TNTAs and react with the adsorbed reactants. However, the photo-generated electrons and holes can recombine easily (Linsebigler et al., 1995). The PEC system in this study can overcome this obstacle by separating the photo-generated electron-hole pairs, with the help of bias potential. The *p-n* junction in BiOI-TNTAs plays a critical role in effectively separating the electron-hole pairs. The conduction band (CB) and valence band (VB) of the BiOI and TNTAs, at the point of zero charge, can be estimated by the following equation (Kim et al., 1993; Lin et al., 2007):

$$E_{VB} = X - E^e + 0.5E_g$$

$$E_{CB} = E_{VB} - E_g$$

where X is the absolute electronegativity of the semiconductor and E^e is the energy of free electrons on the hydrogen scale (ca. 4.5 eV). According to the above equations, the top of the VB and the bottom of the CB of the TNTAs are calculated to be 3.00 and −0.20 eV, respectively. Correspondingly, the VB and CB of BiOI are examined to be 2.25 and 0.63 eV, respectively.

A schematic diagram of the energy band for the p-BiOI and *n*-TNTAs as well as the possible charge separation mechanism after forming the BiOI-TNTAs heterojunction is presented in Fig. 6. Before contact, the conduction band edge of BiOI is more higher than that of TiO_2, and the Fermi level of BiOI is lower than that of TiO_2 (Zhang et al., 2009). After contact, the energy band rises up in BiOI and falls in TNTAs. The Fermi levels of BiOI and the TNTAs achieve an equilibrium as the p-n junction of BiOI and the TNTAs is formed (Yu et al., 2010). BiOI can generate electrons and holes when excited by visible light irradiation. Under irradiation, photo-generated electrons jump to the CB of BiOI, leaving holes in the VB of BiOI. In addition, the photo-generated electrons in the CB of BiOI migrate to the CB of the TNTAs. The photo-generated holes accumulate in the VB of BiOI. The photo-generated electrons transfer from the surface of BiOI to the Ti foil (at the bottom of the TNTAs). Later, the electrons are attracted from the anode (BiOI-TNTAs) to the cathode via the external circuit. In the anodic chamber, the holes could react with H_2O to form hydroxyl radicals (•OH), a strong oxidant, which can oxidize most organic pollutants (Peng et al., 2017). Dong et al. (2015) employed electron ESR to detect •OH in BiOI photocatalytic reaction and proved •OH was responsible for pollutant oxidation. Thus, the *p-n* junction formed in the *p*-BiOI/*n*-TiO_2 interface can separate the photo-generated electron-hole pairs effectively, and reduce the recombination of electron-hole pairs. These separated electrons and holes migrate to the surface and react with the reactants adsorbed on the photocatalyst surfaces, enhancing PEC performance.

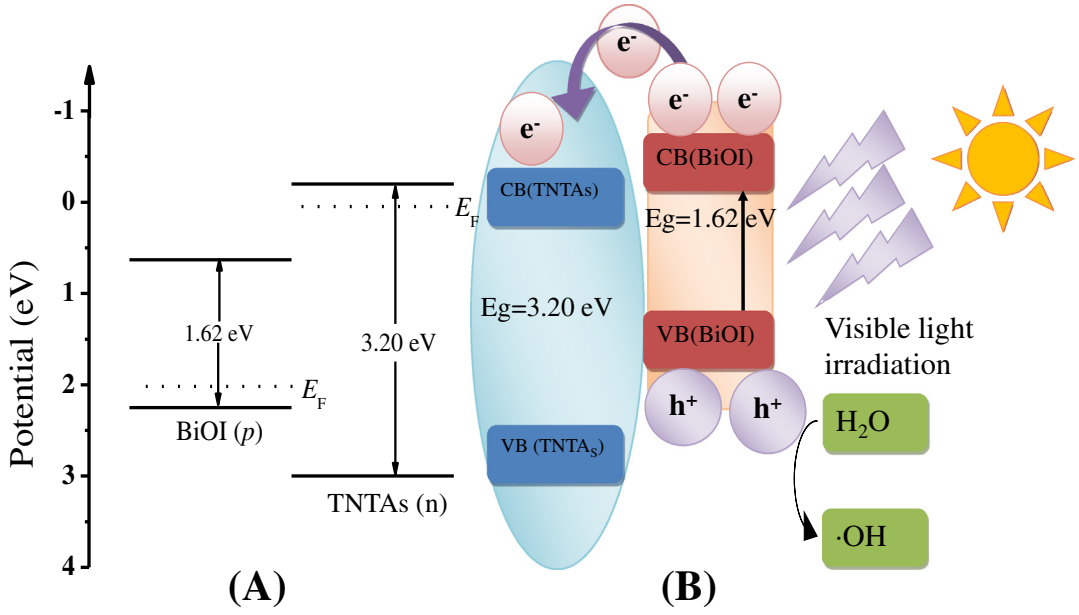

Fig. 6. Schematic diagram for (A) energy bands of BiOI (*p*) and TNTAs (*n*) before contact and (B) formation of a *p-n* junction.

4. Conclusion

BiOI depositing TiO_2 nanotube arrays (BiOI-TNTAs) were successfully synthesized via the CVD method. The as-synthesized BiOI-TNAs were employed as a photo-anode in a self-designed PEC system to simultaneously degrade IBP and generate hydrogen in the anodic and cathodic chambers, respectively. Three different types of photo-anode, TNAs, BiOI-Ti and BiOI-TNTAs, were characterized via SEM, XRD, XPS, UV–vis as well as EIS for better understanding their physical and chemical properties. Among the P, PC, EC and PEC methods, the BiOI-TNTAs PEC process is the most efficient in degrading IBP with a Pseudo-first-order rate constant of 0.0321 min^{-1}. The synergetic effects between electrochemical and photocatalytic contributions in PEC system were quantified by EIS and Bode plot analyses. The electron lifetime (τ_{el}) of BiOI-TNTAs (3.24 ms) was about 4.1 times higher than that of pure TNTAs (0.79 ms) under a bias potential 1.2 V (vs. Ag/AgCl). In the present PEC system, with the contribution of bias potential, most electrons are attracted to the cathode, leading to decreased recombination of photo-generated electrons and holes, thereby enhancing the photocatalytic efficiency.

Acknowledgments

This study was funded by the Ministry of Science and Technology of the Republic of China, Taiwan, for financially supporting this research under Grant No. MOST 105-2221-E-029-001-MY3.

Appendix A. Supplementary data

Supplementary data to this article can be found online at https://doi.org/10.1016/j.scitotenv.2018.03.268.

References

Camacho-Muñoz, D., Martín, J., Santos, J.L., Aparicio, I., Alonso, E., 2010. Occurrence, temporal evolution and risk assessment of pharmaceutically active compounds in Doñana Park (Spain). J. Hazard. Mater. 183 (1–3), 602–608.

Chen, H., Chen, K.-F., Lai, S.-W., Dang, Z., Peng, Y.-P., 2015. Photoelectrochemical oxidation of azo dye and generation of hydrogen via C N co-doped TiO_2 nanotube arrays. Sep. Purif. Technol. 146, 143–153.

Cheng, X., Leng, W., Liu, D., Xu, Y., Zhang, J., Cao, C., 2008. Electrochemical preparation and characterization of surface-fluorinated TiO_2 nanoporous film and its enhanced photoelectrochemical and photocatalytic properties. J. Phys. Chem. C 112 (23), 8725–8734.

Cheng, C., Wang, H., Li, J., Yang, H., Xie, A., Chen, P., Li, S., Huang, F., Shen, Y., 2014. Ordered macroporous CdS-sensitized N-doped TiO_2 inverse opals films with enhanced photoelectrochemical performance. Electrochim. Acta 146, 378–385.

Cole, E.B., Lakkaraju, P.S., Rampulla, D.M., Morris, A.J., Abelev, E., Bocarsly, A.B., 2010. Using a one-electron shuttle for the multielectron reduction of CO_2 to methanol: kinetic, mechanistic, and structural insights. J. Am. Chem. Soc. 132 (33), 11539–11551.

Dai, G., Yu, J., Liu, G., 2011. Synthesis and enhanced visible-light photoelectrocatalytic activity of p−n junction BiOI/TiO_2 nanotube arrays. J. Phys. Chem. C 115 (15), 7339–7346.

Dong, G., Ho, W., Zhang, L., 2015. Photocatalytic NO removal on BiOI surface: the change from nonselective oxidation to selective oxidation. Appl. Catal. B Environ. 168, 490–496.

Grimes, C.A., Mor, G.K., 2009. TiO_2 Nanotube Arrays: Synthesis, Properties, and Applications. Springer.

Hoffmann, M.R., Martin, S.T., Choi, W., Bahnemann, D.W., 1995. Environmental applications of semiconductor photocatalysis. Chem. Rev. 95 (1), 69–96.

Kang, Q., Cao, J., Zhang, Y., Liu, L., Xu, H., Ye, J., 2013. Reduced TiO_2 nanotube arrays for photoelectrochemical water splitting. J. Mater. Chem. A 1 (18), 5766–5774.

Kim, Y.I., Atherton, S.J., Brigham, E.S., Mallouk, T.E., 1993. Sensitized layered metal oxide semiconductor particles for photochemical hydrogen evolution from nonsacrificial electron donors. J. Phys. Chem. 97 (45), 11802–11810.

van de Krol, R., Grätzel, M., 2011. Photoelectrochemical Hydrogen Production. Springer.

Lin, X., Xing, J., Wang, W., Shan, Z., Xu, F., Huang, F., 2007. Photocatalytic activities of heterojunction semiconductors Bi_2O_3/$BaTiO_3$: a strategy for the design of efficient combined photocatalysts. J. Phys. Chem. C 111 (49), 18288–18293.

Linsebigler, A.L., Lu, G., Yates Jr, J.T., 1995. Photocatalysis on TiO_2 surfaces: principles, mechanisms, and selected results. Chem. Rev. 95 (3), 735–758.

Liu, Y., Li, J., Zhou, B., Chen, H., Wang, Z., Cai, W., 2011a. A TiO_2-nanotube-array-based photocatalytic fuel cell using refractory organic compounds as substrates for electricity generation. Chem. Commun. 47 (37), 10314–10316.

Liu, Y., Li, J., Zhou, B., Li, X., Chen, H., Chen, Q., Wang, Z., Li, L., Wang, J., Cai, W., 2011b. Efficient electricity production and simultaneously wastewater treatment via a high-performance photocatalytic fuel cell. Water Res. 45 (13), 3991–3998.

Liu, J.C., Lu, G.H., Xie, Z.X., Zhang, Z.H., Li, S., Yan, Z.H., 2015. Occurrence, bioaccumulation and risk assessment of lipophilic pharmaceutically active compounds in the downstream rivers of sewage treatment plants. Sci. Total Environ. 511, 54–62.

Madhavan, J., Grieser, F., Ashokkumar, M., 2010. Combined advanced oxidation processes for the synergistic degradation of ibuprofen in aqueous environments. J. Hazard. Mater. 178 (1–3), 202–208.

Méndez Arriaga, F., Esplugas, S., Gime'nez, J., 2010. Degradation of the emerging contaminant ibuprofen in water by photo-Fenton. Water Res. 44, 589–595.

Momeni, M.M., Ghayeb, Y., 2015. Visible light-driven photoelectrochemical water splitting on ZnO–TiO_2 heterogeneous nanotube photoanodes. J. Appl. Electrochem. 45 (6), 557–566.

Monfort, O., Pop, L.-C., Sfaelou, S., Plecenik, T., Roch, T., Dracopoulos, V., Stathatos, E., Plesch, G., Lianos, P., 2016. Photoelectrocatalytic hydrogen production by water splitting using $BiVO_4$ photoanodes. Chem. Eng. J. 286, 91–97.

Peng, Y.-P., Yassitepe, E., Yeh, Y.-T., Ruzybayev, I., Shah, S.I., Huang, C., 2012. Photoelectrochemical degradation of azo dye over pulsed laser deposited nitrogen-doped TiO_2 thin film. Appl. Catal. B Environ. 125, 465–472.

Peng, Y.P., Yeh, Y.T., Wang, P.Y., Huang, C., 2013. A solar cell driven electrochemical process for the concurrent reduction of carbon dioxide and degradation of azo dye in dilute $KHCO_3$ electrolyte. Sep. Purif. Technol. 117, 3–11.

Peng, Y.P., Chen, H., Huang, C.P., 2017. The synergistic effect of photoelectrochemical (PEC) reactions exemplified by concurrent perfluorooctanoic acid (PFOA) degradation and hydrogen generation over carbon and nitrogen codoped TiO_2 nanotube arrays (C-N-TNTAs) photoelectrode. Appl. Catal. B Environ. 209, 437–446.

Santos, J.L., Aparicio, I., Alonso, E., 2007. Occurrence and risk assessment of pharmaceutically active compounds in wastewater treatment plants. A case study: Seville city (Spain). Environ. Int. 33, 596–601.

Skoumal, M., Rodríguez, R.M., Cabot, P.L., Centellas, F., Garrido, J.A., Arias, C., Brillas, E., 2009. Electro-Fenton, UVA photoelectro-Fenton and solar photoelectro-Fenton degradation of the drug ibuprofen in acid aqueous medium using platinum and boron-doped diamond anodes. Electrochim. Acta 54, 2077–2085.

Sun, Q., Peng, Y.-P., Chen, H., Chang, K.-L., Qiu, Y.-N., Lai, S.-W., 2016. Photoelectrochemical oxidation of ibuprofen via Cu_2O-doped TiO_2 nanotube arrays. J. Hazard. Mater. 319, 121–129.

Talebian, A., Entezari, M., Ghows, N., 2013. Complete mineralization of surfactant from aqueous solution by a novel sono-synthesized nanocomposite (TiO_2–Cu_2O) under sunlight irradiation. Chem. Eng. J. 229, 304–312.

Tobajas, M., Belver, C., Rodriguez, J., 2016. Degradation of emerging pollutants in water under solar irradiation using novel TiO_2-ZnO/clay nanoarchitectures. Chem. Eng. J. 309, 596–606.

Wang, X., Liu, Y., Zhou, X., Li, B., Wang, H., Zhao, W., Huang, H., Liang, C., Yu, X., Liu, Z., 2012. Synthesis of long TiO_2 nanowire arrays with high surface areas via synergistic assembly route for highly efficient dye-sensitized solar cells. J. Mater. Chem. 22 (34), 17531–17538.

Yang, Y., Zhao, J., Cui, C., Zhang, Y., Hu, H., Xu, L., Pan, J., Li, C., Tang, W., 2016. Hydrothermal growth of ZnO nanowires scaffolds within mesoporous TiO_2 photoanodes for dye-sensitized solar cells with enhanced efficiency. Electrochim. Acta 196, 348–356.

Yao, X., Liu, T., Liu, X., Lu, L., 2014. Loading of CdS nanoparticles on the (101) surface of elongated TiO_2 nanocrystals for efficient visible-light photocatalytic hydrogen evolution from water splitting. Chem. Eng. J. 255, 28–39.

Ye, M., Gong, J., Lai, Y., Lin, C., Lin, Z., 2012. High-efficiency photoelectrocatalytic hydrogen generation enabled by palladium quantum dots-sensitized TiO_2 nanotube arrays. J. Am. Chem. Soc. 134 (38), 15720–15723.

Ye, M., Zheng, D., Lv, M., Chen, C., Lin, C., Lin, Z., 2013. Hierarchically structured nanotubes for highly efficient dye-sensitized solar cells. Adv. Mater. 25 (22), 3039–3044.

Yin, Y., Jin, Z., Hou, F., 2007. Enhanced solar water-splitting efficiency using core/sheath heterostructure CdS/TiO_2 nanotube arrays. Nanotechnology 18 (49), 495–608.

Yu, J.-G., Yu, H.-G., Cheng, B., Zhao, X.-J., Yu, J.C., Ho, W.-K., 2003. The effect of calcination temperature on the surface microstructure and photocatalytic activity of TiO_2 thin films prepared by liquid phase deposition. J. Phys. Chem. B 107 (50), 13871–13879.

Yu, J., Wang, W., Cheng, B., 2010. Synthesis and enhanced photocatalytic activity of a hierarchical porous flowerlike p–n junction NiO/TiO_2 photocatalyst. Chem. Asian. J. 5 (12), 2499–2506.

Yu, Z., Li, F., Sun, L., 2015. Recent advances in dye-sensitized photoelectrochemical cells for solar hydrogen production based on molecular components. Energy Environ. Sci. 8 (3), 760–775.

Zhang, Z., Yuan, Y., Shi, G., Fang, Y., Liang, L., Ding, H., Jin, L., 2007. Photoelectrocatalytic activity of highly ordered TiO_2 nanotube arrays electrode for azo dye degradation. Environ. Sci. Technol. 41 (17), 6259–6263.

Zhang, X., Zhang, L., Xie, T., Wang, D., 2009. Low-temperature synthesis and high visible-light-induced photocatalytic activity of BiOI/TiO_2 heterostructures. J. Phys. Chem. C 113 (17), 7371–7378.

Zhao, X., Zhu, Y., 2006. Synergetic degradation of rhodamine B at a porous $ZnWO_4$ film electrode by combined electro-oxidation and photocatalysis. Environ. Sci. Technol. 40 (10), 3367–3372.

Zhao, X., Qu, J., Liu, H., Hu, C., 2007. Photoelectrocatalytic degradation of triazine-containing azo dyes at γ-Bi_2MoO_6 film electrode under visible light irradiation ($\lambda > 420$ nm). Environ. Sci. Technol. 41 (17), 6802–6807.

Zhou, B., Schulz, M., Lin, H.Y., Shah, S.I., Qu, J.H., Huang, C.P., 2009. Photoeletrochemical generation of hydrogen over carbon-doped TiO_2 photoanode. Appl. Catal. B Environ. 92 (1–2), 41–49.